

CZECH TECHNICAL UNIVERSITY IN PRAGUE,
FACULTY OF ELECTRICAL ENGINEERING

MASTER'S THESIS

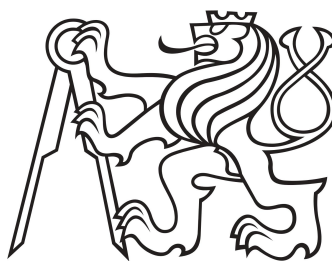
Dual Circularly Polarized Waveguide Antenna

Author

M. ŠIMÁK
DEPARTMENT OF
ELECTROMAGNETIC FIELD

Supervisor

doc. Ing. P. HAZDRA, Ph.D.
DEPARTMENT OF
ELECTROMAGNETIC FIELD



December 2024

[THIS PAGE INTENTIONALLY LEFT BLANK.]

I. Personal and study details

Student's name: **Šimák Martin** Personal ID number: **483523**
Faculty / Institute: **Faculty of Electrical Engineering**
Department / Institute: **Department of Electromagnetic Field**
Study program: **Electronics and Communications**
Specialisation: **Radio Communications and Systems**

II. Master's thesis details

Master's thesis title in English:

Dual Circularly Polarized Waveguide Antenna

Master's thesis title in Czech:

Duálně kruhově polarizovaná vlnovodová anténa

Guidelines:

Research different polarizers in a metallic waveguide, consider round or square transversal shape of the guide. Inspired by circularly polarized patch antenna with chamfered corners, adapt this technique to the waveguide technology (the frequency should be used to be appropriate for easy fabrication, say around 5 GHz). Perform 2D eigenmode analysis of round and square waveguides with inserted metal triangles, and compare the results with the theory of patch antennas of such shapes. Choose one of the waveguide with the polarizer and optimize it to provide the best bandwidth and radiation properties, also design the transition from coaxial cable, preferably with the ability to excite both RHCP and LHCP patterns. Add a small horn (say 15 dBi) to the waveguide and finally optimise the whole structure. Build and measure the whole structure, compare to simulation results.

Bibliography / sources:

- 1/ Polarizers on sections of square waveguides with inner corner ridges | IEEE Conference Publication | IEEE Xplore
- 2/ Compact reconfigurable waveguide circular polarizer | IEEE Conference Publication | IEEE Xplore
- 3/ Design of Wideband Quad-Ridge Waveguide Polarizer | IEEE Conference Publication | IEEE Xplore
- 4/ Optimum-Iris-Set Concept for Waveguide Polarizers | IEEE Journals & Magazine | IEEE Xplore
- 5/ Novel square/rectangle waveguide septum polarizer | IEEE Conference Publication | IEEE Xplore
- 6/ Broadband Septum Polarizer With Triangular Common Port | IEEE Journals & Magazine | IEEE Xplore
- 7/ New Tunable Iris-Post Square Waveguide Polarizers for Satellite Information Systems | IEEE Conference Publication | IEEE Xplore
- 8/ Hexagonal waveguides: New class of waveguides for mm-wave circularly polarized horns | IEEE Conference Publication | IEEE Xplore
- 9/ Hexagonal Waveguide Based Circularly Polarized Horn Antennas for Sub-mm-Wave/Terahertz Band | IEEE Journals & Magazine | IEEE Xplore
- Bow-Tie-Shaped Radiating Element for Single and Dual Circular 10/ Polarization | IEEE Journals & Magazine | IEEE Xplore
- 11/ A Wideband Circularly Polarized Horn Antenna With a Tapered Elliptical Waveguide Polarizer | IEEE Journals & Magazine | IEEE Xplore

Name and workplace of master's thesis supervisor:

doc. Ing. Pavel Hazdra, Ph.D. FEE CTU in Prague, K 13117

Name and workplace of second master's thesis supervisor or consultant:

Date of master's thesis assignment: **04.09.2024**

Deadline for master's thesis submission: _____

Assignment valid until: **15.02.2026**

doc. Ing. Pavel Hazdra, Ph.D.
Supervisor's signature

Head of department's signature

prof., Mgr. Petr Páta, Ph.D.
Dean's signature

III. Assignment receipt

The student acknowledges that the master's thesis is an individual work. The student must produce his thesis without the assistance of others, with the exception of provided consultations. Within the master's thesis, the author must state the names of consultants and include a list of references.

Date of assignment receipt

Student's signature

Contents

Introduction	4
1 Electrodynamics of guided waves	5
1.1 Fundamentals of electrodynamics	5
1.1.1 Maxwell's equations	5
1.1.2 Electromagnetic properties of matter	6
1.1.3 Boundary conditions	8
1.2 Electromagnetic waves	8
1.2.1 The wave equations	8
1.2.2 Monochromatic plane waves	9
1.2.3 Polarization	12
1.2.4 Guided waves	14
2 Polarizer	18
2.1 Principle of operation	18
2.2 Literature survey	19
2.3 Eigenmode analysis	21
2.3.1 Figures of merit	23
2.3.2 Comparison of symmetric waveguides	24
2.4 Square waveguide polarizer	27
2.4.1 Selection of parameters	27
2.4.2 Cross-section tuning	27
2.5 Simulation results	27
2.5.1 Waveguide feed simulation	27
2.5.2 Radiation properties	27
3 Feeding structure	28
3.1 Coaxial-to-waveguide transition	28
3.2 Dual feed	28
3.2.1 Single feed	28

3.2.2	Grating	28
3.2.3	Dual feed optimization	28
4	Antenna	29
4.1	Conical horn	29
4.2	Simulation results	29
5	Assembly	30
5.1	First results	30
5.2	Grating removal	30
5.3	Product finalization	30
5.4	Measurement results	30
	Conclusion	31
	Glossary of Symbols	32
	Bibliography	33
	Index	35

List of Figures

2.1	Polarizers based on symmetric waveguides	21
2.2	Fundamental modes of the symmetric waveguides	22
2.3	Fundamental modes of the symmetric waveguides with metallic inserts .	22
2.4	Circular polarizer cross-section	25
2.5	Square polarizer cross-section	26
2.6	Polarizers – cutoff frequencies	26

Introduction

Lorem ipsum dolor sit amet, consectetur adipiscing elit. Ut purus elit, vestibulum ut, placerat ac, adipiscing vitae, felis. Curabitur dictum gravida mauris. Nam arcu libero, nonummy eget, consectetur id, vulputate a, magna. Donec vehicula augue eu neque. Pellentesque habitant morbi tristique senectus et netus et malesuada fames ac turpis egestas. Mauris ut leo. Cras viverra metus rhoncus sem. Nulla et lectus vestibulum urna fringilla ultrices. Phasellus eu tellus sit amet tortor gravida placerat. Integer sapien est, iaculis in, pretium quis, viverra ac, nunc. Praesent eget sem vel leo ultrices bibendum. Aenean faucibus. Morbi dolor nulla, malesuada eu, pulvinar at, mollis ac, nulla. Curabitur auctor semper nulla. Donec varius orci eget risus. Duis nibh mi, congue eu, accumsan eleifend, sagittis quis, diam. Duis eget orci sit amet orci dignissim rutrum.

Nam dui ligula, fringilla a, euismod sodales, sollicitudin vel, wisi. Morbi auctor lorem non justo. Nam lacus libero, pretium at, lobortis vitae, ultricies et, tellus. Donec aliquet, tortor sed accumsan bibendum, erat ligula aliquet magna, vitae ornare odio metus a mi. Morbi ac orci et nisl hendrerit mollis. Suspendisse ut massa. Cras nec ante. Pellentesque a nulla. Cum sociis natoque penatibus et magnis dis parturient montes, nascetur ridiculus mus. Aliquam tincidunt urna. Nulla ullamcorper vestibulum turpis. Pellentesque cursus luctus mauris.

Synopsis. In chapter 1, Quisque ullamcorper placerat ipsum. Cras nibh. Morbi vel justo vitae lacus tincidunt ultrices. Lorem ipsum dolor sit amet, consectetur adipiscing elit. In hac habitasse platea dictumst. Integer tempus convallis augue. Etiam facilisis. Nunc elementum fermentum wisi. Aenean placerat. Ut imperdiet, enim sed gravida sollicitudin, felis odio placerat quam, ac pulvinar elit purus eget enim. Nunc vitae tortor. Proin tempus nibh sit amet nisl. Vivamus quis tortor vitae risus porta vehicula.

Methodology. Quisque ullamcorper placerat ipsum. Cras nibh. Morbi vel justo vitae lacus tincidunt ultrices. Lorem ipsum dolor sit amet, consectetur adipiscing elit. In hac habitasse platea dictumst. Integer tempus convallis augue. Etiam facilisis. Nunc elementum fermentum wisi. Aenean placerat. Ut imperdiet, enim sed gravida sollicitudin, felis odio placerat quam, ac pulvinar elit purus eget enim. Nunc vitae tortor. Proin tempus nibh sit amet nisl. Vivamus quis tortor vitae risus porta vehicula.

Chapter 1

Electrodynamics of guided waves

This chapter establishes the theoretical foundation for the analysis and design of a waveguide-based antenna system. Beginning with Maxwell's equations and general description of electromagnetic fields in various settings relevant to this work, the wave equations governing guided waves are derived, and their solutions are analysed to elucidate the behaviour of electromagnetic fields within waveguides. This analysis provides a framework for understanding the operation of structures designed in the following chapters. While focusing on the essential elements of waveguide theory, this chapter provides a comprehensive treatment of the subject and establishes the notation used throughout this work.

The exposition endeavours to take inspiration and build upon the foundations laid in [1]–[3], incorporating personal insights and notational preferences to present a cohesive theoretical framework for further chapters.

1.1 Fundamentals of electrodynamics

In this section, the fundamental principles of electromagnetism are presented, starting with Maxwell's equations, which encapsulate the relationships between electric and magnetic fields and their sources. The response of different materials to these fields is then explored through the introduction of *constitutive relations*. Finally, the focus is shifted to the behaviour of electromagnetic fields at material boundaries, providing essential *boundary conditions* for solving electromagnetic problems.

1.1.1 Maxwell's equations

The differential form of Maxwell's equations, as presented below, constitutes the cornerstone of classical electromagnetism, providing a complete¹ framework for analysing electromagnetic phenomena at any point in space and time. These equations summarize the relations between *electric field* \mathbf{E} and *magnetic field* \mathbf{B} and their sources due to charge densities ρ , current densities \mathbf{J} , or the changing of the fields themselves. To ensure the validity of these expressions, let us assume that the field vectors are well-behaved functions, exhibiting continuity and possessing continuous derivatives. This assumption holds for most electromagnetic systems, with exceptions arising at interfaces between distinct media where abrupt changes in charge and current densities may occur.

¹For actual completeness, save for some special properties stemming from interactions in matter, the equations must also be supplemented by the Lorentz's force law $\mathbf{F} = q(\mathbf{E} + \mathbf{v} \times \mathbf{B})$.

$$\nabla \cdot \mathbf{E} = \frac{1}{\epsilon_0} \rho_e, \quad (1.1a)$$

$$\nabla \times \mathbf{E} = -\mu_0 \mathbf{J}_m - \partial_t \mathbf{B}, \quad (1.1b)$$

$$\nabla \cdot \mathbf{B} = \mu_0 \rho_m, \quad (1.1c)$$

$$\nabla \times \mathbf{B} = \mu_0 \mathbf{J}_e + \mu_0 \epsilon_0 \partial_t \mathbf{E}, \quad (1.1d)$$

There is one oddity about equations (1.1) and that is the inclusion of the magnetic charge density ρ_m and magnetic current density \mathbf{J}_m which are part of the ‘generalized concept’. Although these quantities, in spite of diligent search, were never physically observed, their introduction establishes a pleasing balance in Maxwell’s equations while being theoretically sound as well. This concept is further utilized when solving advanced physical problems in applied physics and engineering. This is facilitated by the introduction of equivalent magnetic charge and current which can be used to conveniently express fields as if generated by these fictitious sources, especially in problems where the exact form of the electromagnetic field would otherwise be complicated to elucidate.

Mathematically, equations (1.1), like any differential equations, form a complete problem only when supplemented with suitable boundary conditions in a more traditional sense, such as behaviour of the vector fields ‘in infinity’. These are typically ‘obvious’ from the problem-solving context, e.g., fields vanishing at large distance from localized charge distribution, etc.

1.1.2 Electromagnetic properties of matter

Although Maxwell’s equations in their fundamental form (1.1) provide a complete description of electromagnetic phenomena, an alternative formulation offers a more convenient approach for analysing materials susceptible to electric and magnetic polarization.

Within such media, the total electric charge density ρ_e can be expressed as a sum of the *free charge* density ρ_f , which constitutes the *actual source* charge,² and the *bound charge* $\rho_b = -\nabla \cdot \mathbf{P}$, produced by an electric polarization \mathbf{P} of the material. Moreover, changing electric fields also induce changing polarization, producing *polarization current* $\mathbf{J}_p = \partial_t \mathbf{P}$ which add to the *free current* \mathbf{J}_f . Similarly to electric polarization, a magnetic polarization \mathbf{M} results in a bound current $\mathbf{J}_b = \nabla \times \mathbf{M}$. These effects, inherently connected to the susceptibility of materials to be polarized, hence influence the total electromagnetic field in their vicinity. This led to the introduction of auxiliary field quantities that account for the presence of such media

$$\mathbf{D} = \epsilon_0 (\mathbf{E} + \mathbf{P}), \quad (1.2a)$$

$$\mathbf{H} = \frac{1}{\mu_0} \mathbf{H} - \mathbf{M}. \quad (1.2b)$$

This approach allows for expressing Maxwell’s equations in a form that directly relates the electric and magnetic fields to the free charge and free current, which are sources that can be controlled directly. Using the field quantities defined by equations (1.2), Maxwell’s equations (1.1) read

$$\nabla \cdot \mathbf{D} = \rho_f, \quad (1.3a)$$

$$\nabla \times \mathbf{E} = -\mathbf{J}_m - \partial_t \mathbf{B}, \quad (1.3b)$$

$$\nabla \cdot \mathbf{B} = \rho_m, \quad (1.3c)$$

$$\nabla \times \mathbf{H} = \mathbf{J}_f + \partial_t \mathbf{D}, \quad (1.3d)$$

While equations (1.3) effectively express electromagnetic laws within media, their

²It is important to reinforce the idea that the magnetic charge and current are fictitious ‘source’ quantities. Therefore, they are already, by definition, purely *free* quantities.

hybrid notation, involving both \mathbf{E} and \mathbf{D} , and both \mathbf{B} and \mathbf{H} , necessitates the use of *constitutive relations*. These relations, which establish correspondence between the respective electric and magnetic field quantities, are material-dependent and reflect the specific response of a medium to electric and magnetic fields. In general, these relationships can be expressed as

$$\mathbf{D} = \hat{\epsilon} * \mathbf{E}, \quad (1.4a)$$

$$\mathbf{B} = \hat{\mu} * \mathbf{H}, \quad (1.4b)$$

where $\hat{\epsilon}$ and $\hat{\mu}$ are the material's *permittivity* and *permeability*, respectively, and the asterisk denotes *convolution*.

Remark 1.1.1. In formulations akin to equations (1.3), with emphasis on the separation of free and bound sources, some authors prefer to further dissect the free current, too. This current is generally conceptualized as the current 'not directly tied to the bound charges' within a material. To name a few commonly recognized, *convection current*, *beam current*, or *conduction current*. It is the conduction current which is, in electrical engineering, especially worth mentioning because it arises from the movement of charges, typically electrons, that can move freely throughout the material. This kinetic energy of charges in conductors is the main cause of losses in waveguides and can be expressed by

$$\mathbf{J}_c = \hat{\sigma} * \mathbf{E}, \quad (1.5)$$

where $\hat{\sigma}$ is the material's *conductivity*. Equation (1.5), together with equations (1.4), completes the required set of constitutive relations.

The *constitutive parameters* $\hat{\epsilon}$, $\hat{\mu}$, and $\hat{\sigma}$, generally represented as complex second-rank tensors, establish the relationship between the applied electromagnetic fields and the material's response. The functional dependencies of these tensors provide a classification scheme for material properties:

- *Linearity:* A material is classified as linear if its constitutive parameters are independent of the applied field strength; otherwise, it is considered nonlinear.
- *Homogeneity:* If the constitutive parameters are invariant with respect to position within the material, it is deemed homogeneous; conversely, spatial dependence indicates an inhomogeneous medium.
- *Isotropy:* Materials exhibiting constitutive parameters independent of the applied field's direction are classified as isotropic. Conversely, direction-dependent parameters signify an anisotropic material, with crystals being a prime example.
- *Dispersion:* Materials whose constitutive parameters exhibit frequency dependence are categorized as dispersive. While some materials demonstrate negligible frequency dependence and can be effectively considered nondispersive, all materials encountered in practice exhibit some degree of dispersion.

Example 1.1.2 [Constitutive relations in free space]. In the simplest case of free space, equations (1.4a), (1.4b), and (1.5) become

$$\hat{\epsilon} = \epsilon_0 \approx 8.854 \times 10^{-12} \text{ F m}^{-1}, \quad (1.6a)$$

$$\hat{\mu} = \mu_0 = 4\pi \times 10^{-7} \text{ H m}^{-1}, \quad (1.6b)$$

$$\hat{\sigma} = \sigma_0 = 0 \text{ S m}^{-1}. \quad (1.6c)$$

1.1.3 Boundary conditions

While the differential form of Maxwell's equations is a powerful tool for analysing electromagnetic fields within continuous media, material boundaries introduce discontinuities that require special treatment. These discontinuities in the fields arise at interfaces between media with different electrical properties or at surfaces carrying charge or current densities. To accurately describe the behaviour of the fields across such boundaries, Maxwell's equations in their integral form, which naturally incorporate these discontinuities, are more convenient. This form is obtained by applying integral theorems from vector calculus to equations (1.3) which then take on the form of

$$\oint_S \mathbf{D} \cdot d\mathbf{a} = Q_e, \quad (1.7a)$$

$$\oint_{\partial S} \mathbf{E} \cdot dl = - \int_S \mathbf{J}_m \cdot d\mathbf{a} - \frac{d}{dt} \int_S \mathbf{B} \cdot d\mathbf{a}, \quad (1.7b)$$

$$\oint_S \mathbf{B} \cdot d\mathbf{a} = Q_m, \quad (1.7c)$$

$$\oint_{\partial S} \mathbf{H} \cdot dl = \int_S \mathbf{J}_e \cdot d\mathbf{a} + \frac{d}{dt} \int_S \mathbf{D} \cdot d\mathbf{a}, \quad (1.7d)$$

where S is any closed surface.

Consider a boundary between two different media. The first medium is characterized by permittivity ϵ_1 and permeability μ_1 , while the second medium is characterized by permittivity ϵ_2 and permeability μ_2 . At this interface, electric and magnetic surface charge densities, denoted by q_f and q_m , respectively, may be present. Additionally, electric and magnetic surface current densities, denoted by j_f and j_m , respectively, may also exist. The general *boundary conditions* for electrodynamics are then obtained by applying equations (1.7) to arbitrary surfaces encompassing a portion of the interface, yielding

$$\mathbf{e}_n \cdot (\mathbf{D}_1 - \mathbf{D}_2) = q_f, \quad (1.8a)$$

$$-\mathbf{e}_n \times (\mathbf{E}_1 - \mathbf{E}_2) = j_m, \quad (1.8b)$$

$$\mathbf{e}_n \cdot (\mathbf{B}_1 - \mathbf{B}_2) = q_m, \quad (1.8c)$$

$$\mathbf{e}_n \times (\mathbf{H}_1 - \mathbf{H}_2) = j_f. \quad (1.8d)$$

1.2 Electromagnetic waves

Having established the foundations of electromagnetism, the focus is now shifted to one of its most significant consequences: the existence of electromagnetic waves. In this section, the manner in which Maxwell's equations predict the propagation of these waves is explored. The wave equations for the electric and magnetic fields are derived, revealing their interconnected nature and their ability to sustain each other even in the absence of sources. Subsequently, the simplest and most fundamental solutions to these equations, *monochromatic plane waves*, are investigated. Finally, the confinement and guidance of these plane waves within conducting cavities is examined, laying the groundwork for understanding waveguides and resonant structures.

1.2.1 The wave equations

Maxwell's equations provide a comprehensive description of electromagnetic phenomena, but their coupled nature can make them challenging to solve directly. To

facilitate analysis, particularly in source-free regions, it's often advantageous to decouple the equations and express them in terms of the electric and magnetic fields individually. Inside regions with no *free* charge or *free* current, Maxwell's equations (1.3) take on the form of

$$\nabla \cdot \mathbf{D} = 0, \quad (1.9a)$$

$$\nabla \times \mathbf{E} = -\partial_t \mathbf{B}, \quad (1.9b)$$

$$\nabla \cdot \mathbf{B} = 0, \quad (1.9c)$$

$$\nabla \times \mathbf{H} = \sigma \mathbf{E} + \partial_t \mathbf{D}. \quad (1.9d)$$

Furthermore, if the medium is *linear* and *homogeneous*, equation (1.9d) can be fully expressed in terms of \mathbf{E} . With this simplification, applying the curl to equations (1.9b) and (1.9d) yields

$$\Delta \mathbf{E} = \mu \sigma \partial_t \mathbf{E} + \mu \epsilon \partial_t^2 \mathbf{E}, \quad (1.10a)$$

$$\Delta \mathbf{B} = \mu \sigma \partial_t \mathbf{B} + \mu \epsilon \partial_t^2 \mathbf{B}. \quad (1.10b)$$

Therefore, electric and magnetic fields in linear homogeneous media both clearly satisfy the wave equation with a linear damping term $\mu \sigma \partial_t$, introduced by conductive losses. Moreover, in regions with $\sigma = 0$, such as free space or ideal insulators, equations (1.10) simplify even more to

$$\Delta \mathbf{E} = \mu \epsilon \partial_t^2 \mathbf{E}, \quad (1.11a)$$

$$\Delta \mathbf{B} = \mu \epsilon \partial_t^2 \mathbf{B}, \quad (1.11b)$$

taking on the form of classical wave equations which are ubiquitous in physics. This also immediately gives rise to the formula

$$v = \frac{1}{\sqrt{\epsilon \mu}} = \frac{c}{\sqrt{\epsilon_r \mu_r}} \quad (1.12)$$

for the speed of electromagnetic waves in linear homogeneous media.

Remark 1.2.1. Compared with the original Maxwell's equations (1.3), these equations form two systems of second-order partial differential equations but are now decoupled and provide us with an additional solving method for given boundary-value problems. However, it is important to note that the wave equations (1.10a) and (1.10b) were derived from Maxwell's equations (1.9) by differentiation. This impedes their mathematical equivalence. More specifically, as stated in [2], whereas every solution to Maxwell's equations is also a solution for the wave equations, the converse is not true.

1.2.2 Monochromatic plane waves

The electromagnetic theory presented thus far describes general vector fields that vary in space and time. However, as shown in section 1.2.1, electromagnetic fields in source-free regions exhibit wave behaviour. Nonetheless, these time-varying vector fields remain complex and challenging to analyse in practical systems. Consider the elementary solution to the wave equation

$$\hat{\psi}(\mathbf{r}, t) = \hat{\Psi}_0 \exp \left[i \left(\hat{\mathbf{k}} \cdot \mathbf{r} - \omega t \right) \right]. \quad (1.13)$$

Here, $\hat{\mathbf{k}}$ is the complex *wave vector* indicating the direction of wave propagation, and ω is the angular frequency of the wave. Equation (1.13) is expressed in terms of a *complex wave function* with a *complex amplitude* $\hat{\Psi}_0 \equiv \Psi_0 e^{i\delta}$. This quantity encapsulates both the *real amplitude* Φ_0 and the *phase shift* δ , of the physical wave. A sinusoidal wave

representing this solution in physical reality can be extracted from equation (1.13) using the *Euler's formula*, yielding

$$\psi(\mathbf{r}, t) = \operatorname{Re} [\hat{\Psi}_0 \exp [i(\hat{\mathbf{k}} \cdot \mathbf{r} - \omega t + \delta)]] = \operatorname{Re} [\hat{\psi}(\mathbf{r}, t)]. \quad (1.14)$$

Remark 1.2.2. Clearly, if equation (1.14) satisfies equations (1.11) and Maxwell's equations, the same holds true for equation (1.13), as the imaginary part differs from the real part only by the replacement of sine with cosine.

Equation (1.13) serves as an established elementary solution to the general wave equation, and hence also to equations (1.11). Substituting this solution into equations (1.10), it becomes evident that these 'lossy wave equations' also admit plane-wave solutions. Furthermore, this substitution allows for the derivation of a general formula for the complex *wavenumber*

$$\hat{k}^2 = \hat{\mathbf{k}} \cdot \hat{\mathbf{k}} = \mu\epsilon\omega^2 + i\mu\sigma\omega. \quad (1.15)$$

In the context of equation (1.13), it is evident that the real part of the complex wavenumber \hat{k} is the *actual* wavenumber as it determines the change of phase with spatial propagation. For this reason, the real part is simply denoted k and is called the *phase constant*. In contrast, the imaginary part of \hat{k} is responsible for the exponential damping, or attenuation, in conductive media, and hence is called the *attenuation constant*.

Waves described by equation (1.13) are called *monochromatic*, or *time-harmonic*, *plane* waves. Monochromaticity refers to the fact that the wave oscillates at a single frequency ω through time, while planarity indicates that the fields are uniform over every plane perpendicular to the direction of propagation. Although less common, plane waves could alternatively be called *space-harmonic*,³ as both of these terms signify a sinusoidal dependence on a given variable. In the case of monochromaticity, the variable is time, oscillating with an angular frequency ω . Similarly, planarity reflects the waveform repetition in the spatial coordinates, projected into the propagation direction, with a well-defined spatial frequency k .

The significance of this particular solution stems from the fact that, in practice, any wave we will be dealing with can be expressed as a linear combination of these monochromatic plane waves, i.e.,

$$\hat{\psi}(\mathbf{r}, t) = \int_{\mathbb{R}^3} \hat{\Psi}_0(\mathbf{k}) \exp [i(\hat{\mathbf{k}} \cdot \mathbf{r} - \omega t)] d\mathbf{k}. \quad (1.16)$$

This superposition principle mathematically reflects the Fourier transform over every plane wave corresponding to a given frequency ω . With this formally sound mathematical description, the existence of a unique linear combination for 'any wave we will be dealing with', as vaguely stated above, can be rigorously established.

Indeed, since any physically realizable signal is square-integrable and has compact support,⁴ the existence of its Fourier transform is guaranteed. This implication is granted by recalling that the combination of square-integrability and compact support implies, by the Cauchy-Schwarz inequality, absolute integrability which forms a sufficient condition for the existence of the Fourier transform. Therefore, any such physical signal

³Therefore, monochromatic plane waves are something one could call *spacetime-harmonic* or simply *harmonic*.

⁴In the field of signal processing, these signal properties are often described as having *finite energy* and *duration*, respectively.

can be confidently decomposed into a superposition of monochromatic plane waves, as expressed in equation equation (1.16). This decomposition into a unique linear combination of plane waves of different frequencies underpins much of the mathematical theory concerning Fourier analysis. For a deeper dive into the mathematical foundations of Fourier integrals, [4] can be consulted. Furthermore, a formulation of Dirichlet conditions which are more attuned to signal processing applications can be found in [5].

Because the focus of this text is confined to signals that are physically realizable and thus possess these crucial properties, a restriction of our attention to monochromatic plane waves is justified. Therefore, fields taking on the form of

$$\hat{\mathbf{E}}(\mathbf{r}, t) = \hat{\mathbf{E}}_0 \exp \left[i \left(\hat{\mathbf{k}} \cdot \mathbf{r} - \omega t \right) \right], \quad (1.17a)$$

$$\hat{\mathbf{B}}(\mathbf{r}, t) = \hat{\mathbf{B}}_0 \exp \left[i \left(\hat{\mathbf{k}} \cdot \mathbf{r} - \omega t \right) \right] \quad (1.17b)$$

are considered, where $\hat{\mathbf{E}}_0$ and $\hat{\mathbf{B}}_0$ are complex amplitudes.

As discussed in remark 1.2.1, satisfying the wave equations does not guarantee solutions to Maxwell's equations. Substituting the solutions of the wave equations into Maxwell's equations is necessary, as it might refine the solutions or yield more information. As an example, consider the plane waves in vacuum.

Example 1.2.3 [Monochromatic plane waves in free space]. Substituting equations (1.17a) and (1.17b) for the electric and magnetic field in the free-space version of equations (1.9a) and (1.9c) read

$$\mathbf{k} \cdot \hat{\mathbf{E}}_0 = \mathbf{k} \cdot \hat{\mathbf{B}}_0 = 0, \quad (1.18)$$

i.e., the electromagnetic fields are *transverse*. Furthermore, either of equations (1.9b) and (1.9d) yields

$$\hat{\mathbf{B}}_0 = \frac{1}{\omega} (\mathbf{k} \times \hat{\mathbf{E}}_0) = \frac{1}{c} (\mathbf{e}_k \times \hat{\mathbf{E}}_0). \quad (1.19)$$

Clearly, in free space, \mathbf{E} and \mathbf{B} are *mutually perpendicular* and *in phase*, meaning their oscillations reach their peaks and troughs simultaneously.

To further characterize the plane wave, a *polarization vector* is introduced. This unit vector points in the direction of electric field oscillations, i.e.,

$$\mathbf{e}_n \cdot \mathbf{E} = \mathbf{E} \quad \|\mathbf{e}_n\| = 1. \quad (1.20)$$

With this definition, the complete solution to Maxwell's equations for a plane wave in free space takes the form of

$$\mathbf{E}(\mathbf{r}, t) = E_0 \cos(\mathbf{k} \cdot \mathbf{r} - \omega t + \delta) \mathbf{e}_n, \quad (1.21)$$

$$\mathbf{B}(\mathbf{r}, t) = \frac{1}{c} E_0 \cos(\mathbf{k} \cdot \mathbf{r} - \omega t + \delta) (\mathbf{k} \times \mathbf{e}_n). \quad (1.22)$$

It's important to note that this transversality of the electromagnetic fields is a specific property of plane waves in free space or lossless media. When waves are confined in waveguides or propagate through lossy media, the fields generally have longitudinal components as well. This distinction arises because the boundary conditions imposed by the waveguide or the interactions with the medium can alter the field structure.

1.2.3 Polarization

A brief examination of the general polarization properties of monochromatic plane waves is now undertaken. For the sake of simplicity, consideration is restricted to propagation within a vacuum. Consequently, the Cartesian coordinate system is aligned such that the unit vector e_z coincides with the unit vector e_k which defines the direction of propagation. The remaining real unit vectors, e_x and e_y , are then defined such that (e_x, e_y, e_z) constitutes a right-handed orthogonal triad of unit vectors. Thus, the ordered set of vectors (e_x, e_y) forms a basis for the complex amplitude of the electric field \mathbf{E} , and the electric field can thereby be expressed as

$$\hat{\mathbf{E}}(\mathbf{r}, t) = [\hat{E}_x \mathbf{e}_x + \hat{E}_y \mathbf{e}_y] \exp [i\phi(\mathbf{r}, t)], \quad (1.23)$$

where

$$\hat{E}_x = E_x \exp(i\delta_x), \quad \hat{E}_y = E_y \exp(i\delta_y), \quad (1.24)$$

for some real numbers E_x , E_y , δ_x , and δ_y , and

$$\phi(\mathbf{r}, t) = \hat{\mathbf{k}} \cdot \mathbf{r} - \omega t. \quad (1.25)$$

Expressing the real part of equation (1.23) yields

$$\text{Re} [\hat{\mathbf{E}}] = E_x \cos(\phi + \delta_x) \mathbf{e}_x + E_y \cos(\phi + \delta_y) \mathbf{e}_y = A_x \mathbf{e}_x + A_y \mathbf{e}_y. \quad (1.26)$$

Equating the components from the second relation in equation (1.26) and applying goniometric identities, the following relationships are obtained:

$$\frac{A_x}{E_x} \sin(\delta_y) - \frac{A_y}{E_y} \sin(\delta_x) = \sin(\delta_y - \delta_x) \cos(\phi), \quad (1.27a)$$

$$\frac{A_x}{E_x} \sin(\delta_y) - \frac{A_y}{E_y} \sin(\delta_x) = \sin(\delta_y - \delta_x) \cos(\phi). \quad (1.27b)$$

Subsequent squaring and addition of equations (1.27a) and (1.27b) yields

$$\left(\frac{A_x}{E_x} \right)^2 + \left(\frac{A_y}{E_y} \right)^2 - 2 \frac{A_x}{E_x} \frac{A_y}{E_y} \cos(\delta) = \sin^2(\delta), \quad (1.28)$$

where $\delta \equiv \delta_y - \delta_x$. Clearly, equation (1.28) defines an ellipse in the plane transverse to the propagation direction. Accordingly, it can be stated that the general monochromatic plane wave described in equation (1.13) exhibits *elliptical polarization*. The eccentricity and orientation of the ellipse are related to the phase difference δ and the amplitude ratio E_y/E_x . Inspecting equation (1.28), two special types of polarization can be identified for specific parameter values.

Linear polarization. The first situation arises when the polarization ellipse degenerates into a straight line. This condition occurs when the electric field components are either in-phase or out-of-phase by half-wavelength, i.e.,

$$\delta = \delta_y - \delta_x = m\pi, \quad m \in \mathbb{N}_0. \quad (1.29)$$

This situation corresponds to *linear polarization* and equation (1.26) is rendered as

$$\text{Re} [\hat{\mathbf{E}}(\mathbf{r}, t)] = [E_x \mathbf{e}_x \pm E_y \mathbf{e}_y] \cos(\phi + \delta_x). \quad (1.30)$$

Circular polarization. The alternative scenario arises when the polarization ellipse simplifies into a circle. This simplification occurs exclusively when the orthogonal electric field components possess equal amplitude and are out-of-phase by one-quarter wavelength, i.e.,

$$E_x = E_y = \frac{E}{\sqrt{2}}, \quad \delta = \delta_y - \delta_x = (2m + 1)\frac{\pi}{2}, \quad m \in \mathbb{Z}. \quad (1.31)$$

This condition corresponds to *circular polarization*, as the tip of the polarization vector traces a circle within every fixed transverse plane. To ascertain the direction of circular movement, the plane $z = 0$ is considered. By setting $\delta_x = 0$,⁵ equation (1.26) is expressed as

$$\text{Re} [\hat{\mathbf{E}}_{\pm}(\mathbf{0}, t)] = \frac{E}{\sqrt{2}} [\cos(\omega t) \mathbf{e}_x \pm \sin(\omega t) \mathbf{e}_y]. \quad (1.32)$$

This expression demonstrates that, when viewed from the direction defined by $\hat{\mathbf{k}}$, the electric field $\hat{\mathbf{E}}^+$ represents a circularly polarized wave with the polarization vector rotating anticlockwise, thus defining *left-hand circular polarization* (LHCP). Conversely, the case of $\hat{\mathbf{E}}^-$ represents a circularly polarized wave with the polarization vector rotating clockwise, defining *right-hand circular polarization* (RHCP).

The exposition given so far is aligned with Augustin-Jean Fresnel's general definition of elliptical polarization, as presented in his memoir to the French Academy of Sciences on 9 December 1822, wherein the concepts of the three types of polarization—general elliptical polarization, and its specific forms, linear and circular polarization—were coined. The following remark, however, provides an alternative, and often advantageous, approach.

Remark 1.2.4 [Complex basis for circular polarization]. For the electric field decomposition basis, the following complex conjugate vectors, rather than the Cartesian vectors \mathbf{e}_x and \mathbf{e}_y , are now considered:

$$\mathbf{e}_+ = \frac{1}{\sqrt{2}} (\mathbf{e}_x + i\mathbf{e}_y), \quad \mathbf{e}_- = \frac{1}{\sqrt{2}} (\mathbf{e}_x - i\mathbf{e}_y). \quad (1.33)$$

These vectors maintain orthonormality. Using this basis, it is evident that the real part of the thus formed complex electric field

$$\hat{\mathbf{E}}_{\pm}(\mathbf{r}, t) = E \mathbf{e}_{\pm} \exp [i(\hat{\mathbf{k}} \cdot \mathbf{r} - \omega t)] = \frac{E}{\sqrt{2}} [\mathbf{e}_x \pm i\mathbf{e}_y] \exp [i(\hat{\mathbf{k}} \cdot \mathbf{r} - \omega t)], \quad (1.34)$$

evaluated at $\mathbf{r} = 0$, is equivalent to equation (1.32). Because the ordered set of vectors defined by equation (1.33) constitutes a valid basis for the transverse plane, analogous to the $(\mathbf{e}_x, \mathbf{e}_y)$ basis, the expression

$$\hat{\mathbf{E}} = [E_+ \mathbf{e}_+ + E_- \mathbf{e}_-] \exp [i\phi] \quad (1.35)$$

is an equivalent representation to equation (1.23). Consequently, any monochromatic plane wave can be decomposed into RHCP and LHCP components, in a manner analogous to its decomposition into orthogonal linearly polarized components.

⁵The choice $\delta_x = 0$ is inconsequential to the resulting polarization as it depends only on the phase difference δ .

1.2.4 Guided waves

The behaviour of electromagnetic waves within a waveguide is now explored. To provide a clear framework for analysis, it is assumed that the waveguide walls are perfect electric conductors (PEC), implying the absence of surface sources. This idealization leads to specific boundary conditions

$$\mathbf{e}_n \times \mathbf{E} = 0, \quad (1.36a)$$

$$\mathbf{e}_n \cdot \mathbf{B} = 0. \quad (1.36b)$$

It is important to recognize that free charges and currents will be induced on the surface precisely to enforce these constraints.

Furthermore, the focus is placed on monochromatic plane waves propagating along the waveguide. This implies that the electric and magnetic fields have a harmonic time dependence with a single angular frequency ω . The $\hat{\cdot}$ notation is dispensed with as \hat{k} is real for the cases of interest. The general form of the fields is then given by equations (1.17) where the z -axis is aligned with the waveguide's longitudinal direction. The complex amplitudes of the fields,

$$\hat{\mathbf{E}}_0 = E_x \mathbf{e}_x + E_y \mathbf{e}_y + E_z \mathbf{e}_z, \quad (1.37a)$$

$$\hat{\mathbf{B}}_0 = B_x \mathbf{e}_x + B_y \mathbf{e}_y + B_z \mathbf{e}_z, \quad (1.37b)$$

are functions of the transverse coordinates, x and y , reflecting the spatial variations of the fields within the waveguide cross-section.

To further simplify the analysis, the waveguide is considered to be source-free, meaning that there are no free charges or currents *impressed* within the waveguide itself. This allows the utilization of the simplified form of Maxwell's equations (1.9). Due to the assumed linearity of the medium within the waveguide, these equations are expressed in terms of E and B .

With these assumptions in place, the wave behaviour within the waveguide can be analysed. From equations (1.9b) and (1.9d), adapted for a linear medium, a set of coupled differential equations relating the transverse components of the electric and magnetic fields is obtained. These equations can be solved to express the transverse field components in terms of the longitudinal components, taking the form of

$$E_x = \zeta (k \partial_x E_z + \omega \partial_y B_z), \quad (1.38a)$$

$$B_x = \zeta \left(k \partial_x B_z - \frac{\omega}{c^2} \partial_y E_z \right), \quad (1.38c)$$

$$E_y = \zeta (k \partial_y E_z - \omega \partial_x B_z), \quad (1.38b)$$

$$B_y = \zeta \left(k \partial_y B_z + \frac{\omega}{c^2} \partial_x E_z \right), \quad (1.38d)$$

where $\zeta = i/((\omega/c)^2 - k^2)$. Finally, substituting equations (1.38) into equations (1.9a) and (1.9c) leads to uncoupled equations

$$\left[\partial_x^2 + \partial_y^2 + \left(\frac{\omega}{c} \right)^2 - k^2 \right] E_z = 0, \quad (1.39a)$$

$$\left[\partial_x^2 + \partial_y^2 + \left(\frac{\omega}{c} \right)^2 - k^2 \right] B_z = 0. \quad (1.39b)$$

These equations, often referred to as the *Helmholtz equations*, govern the longitudinal field components and play a crucial role in determining the allowed modes of propagation within the waveguide. These modes are categorized based on the presence or absence of longitudinal components in the electric and magnetic fields. *Transverse electric* (TE) waves have $E_z = 0$, while *transverse magnetic* (TM) waves have $B_z = 0$. The simplest waves, with both $E_z = B_z = 0$ are called *transverse electromagnetic* (TEM) waves, but these cannot exist within a hollow waveguide due to boundary conditions.

Remark 1.2.5 [Non-existence of TEM waves in hollow waveguides]. To further illustrate this point, consider the case of a waveguide with perfectly conducting walls.

Beginning with the scenario where the longitudinal component of the electric field, E_z , is zero, it follows from equation (1.9a) that the divergence of the electric field in the transverse plane must also be zero. Similarly, when the longitudinal component of the magnetic field, B_z , is zero, equation (1.9b) dictates that the curl of the electric field in the transverse plane must vanish.

Combining these results, the complex amplitude of the electric field, $\hat{\mathbf{E}}_0$, can be expressed as the gradient of a scalar potential φ that satisfies the Laplace's equation $\Delta\varphi = 0$. However, the boundary condition on the electric field, as expressed in equation (1.36a), enforces an equipotential at the conductor surface. Since Laplace's equation admits no local extrema, the potential must be constant throughout the waveguide, leading to a zero electric field.

Remark 1.2.6 [Modal decomposition of guided waves]. The equations for E_z and B_z , equations (1.39), are instances of the *Helmholtz equation* with Dirichlet and Neumann boundary conditions, respectively. This mathematical structure the eigenvalue problem for the Laplace operator arising in various physical contexts.

For instance, the same equation and boundary conditions govern the vertical displacements of a vibrating drumhead. In this analogy, TM modes correspond to a drumhead with fixed boundaries, while TE modes correspond to a drumhead with free boundaries. The TM case is also isomorphic to the Schrödinger problem for the wave functions and energy eigenvalues of a free particle in a two-dimensional box with hard walls. Seeking inspiration in these analogous problems provides useful intuition when thinking about the modal eigenfunctions and eigenvalues of a waveguide. Some key mathematical results stemming from these analogies include:

- (a) There are an infinite number of TE- and TM-mode eigenfunctions.
- (b) The eigenvalues are all real and positive.
- (c) The eigenfunctions can always be chosen real.
- (d) The eigenfunctions form a complete set of functions.
- (e) Eigenfunctions belonging to different eigenvalues are orthogonal, i.e.,

$$\int_S \left[\hat{\mathbf{E}}_{0,\alpha} \times \hat{\mathbf{B}}_{0,\beta}^* \right] dS = C\delta_{\alpha\beta}, \quad (1.40)$$

where S is an arbitrary waveguide cross-section and $\delta_{\alpha\beta}$ is the Kronecker's delta distribution.

Perhaps the most significant result in terms of applied electrodynamics is the completeness of the eigenfunctions, which implies that any field within a waveguide can be composed of its modes. Specifically, if α denotes a distinct mode⁶ then any wave travelling in the positive direction (denoted by the + superscript) can be decomposed as

$$\hat{\mathbf{E}}^+ = \sum_{\alpha} C_{\alpha}^+ \left[\hat{\mathbf{E}}_{0,\alpha} + \mathbf{e}_z E_{z,\alpha} \right] \exp(-ik_{\alpha} z), \quad (1.41)$$

$$\hat{\mathbf{B}}^+ = \sum_{\alpha} C_{\alpha}^+ \left[\hat{\mathbf{B}}_{0,\alpha} + \mathbf{e}_z B_{z,\alpha} \right] \exp(-ik_{\alpha} z). \quad (1.42)$$

⁶For example, in the case of a rectangular waveguide, a mode is given by the combination of two integers, m and n .

Similarly, for the negative direction (denoted by the $-$ superscript), the decomposition is given by

$$\hat{\mathbf{E}}^- = \sum_{\alpha} C_{\alpha}^- \left[\hat{\mathbf{E}}_{0,\alpha} - \mathbf{e}_z E_{z,\alpha} \right] \exp(i k_{\alpha} z), \quad (1.43)$$

$$\hat{\mathbf{B}}^- = \sum_{\alpha} C_{\alpha}^- \left[-\hat{\mathbf{B}}_{0,\alpha} + \mathbf{e}_z B_{z,\alpha} \right] \exp(i k_{\alpha} z). \quad (1.44)$$

Furthermore, thanks to the mutual orthogonality of modes, the modal decomposition is uniquely given by the orthogonal projection

$$C_{\alpha}^{\pm} = \frac{1}{2} \frac{\int_S \left[\hat{\mathbf{E}}_{0,\alpha}^* \cdot \hat{\mathbf{E}} \pm \left(\frac{\omega}{k_{\alpha}} \right)^2 \hat{\mathbf{B}}_{0,\alpha}^* \cdot \hat{\mathbf{B}} \right] dS}{\int_S \hat{\mathbf{E}}_{0,\alpha}^* \cdot \hat{\mathbf{E}}_{0,\alpha} dS} \exp(\pm i k_{\alpha} z), \quad (1.45)$$

where S is an arbitrary cross-section of the waveguide.

These two results combined lead to a powerful conclusion: the tangential fields within an arbitrary cross-section of the waveguide fully determine the field everywhere within the waveguide. This means that if the tangential components of the electric and magnetic fields are known on a single transverse plane, the entire field distribution within the waveguide can be uniquely determined, both in the transverse plane and along the direction of propagation.

Example 1.2.7 [TE waves in a rectangular waveguide]. This example delves into the specific case of TE waves within a rectangular waveguide. A waveguide with height a in the x -direction and width b in the y -direction is considered, the z -axis again being aligned with the waveguide's longitudinal direction. The objective is to derive an expression for the longitudinal component of the magnetic field, B_z , using the method of separation of variables. This method involves assuming that, for every x and y , $B_z(x, y)$ can be expressed as the product of two independent functions, $X(x)$ and $Y(y)$.

Substituting this product into equation (1.39b) yields a differential equation that can be rearranged by dividing through by B_z . This rearranged equation reveals that the x -dependent and y -dependent terms must be constant, leading to two ordinary differential equations,

$$\frac{1}{X} X'' = -k_x^2, \quad (1.46a)$$

$$\frac{1}{Y} Y'' = -k_y^2. \quad (1.46b)$$

Additionally, a relationship between the separation constants, k_x and k_y , and the wave number, k , is established as

$$-k_x^2 - k_y^2 + \left(\frac{\omega}{c} \right)^2 - k^2 = 0. \quad (1.47)$$

Equation (1.46a) is a simple second-order ordinary differential equation, with a general solution of the form

$$X(x) = A \sin(k_x x) + B \cos(k_x x). \quad (1.48)$$

To determine the particular solution, boundary conditions must be applied. The boundary condition (1.36b) enforces the vanishing of B_x at $x = 0$ and $x = a$. According

to equation (1.38c), this translates to enforcing the vanishing of $\partial_x B_z = X'$ at those points. This implies $A = 0$ and the separation constant k_x must satisfy the condition

$$k_x = \frac{m\pi}{a}, \quad m \in \mathbb{N}_0. \quad (1.49)$$

Similarly, for the function $Y(y)$, the boundary condition leads to the condition

$$k_y = \frac{n\pi}{b}, \quad n \in \mathbb{N}_0. \quad (1.50)$$

Combining these results, the particular solution for B_z takes the form of

$$B_z(x, y) = B_0 \cos\left(\frac{m\pi}{a}x\right) \cos\left(\frac{n\pi}{b}y\right), \quad (1.51)$$

representing the TE_{mn} wave with the corresponding wavenumber given by equation (1.47). This information is a complete solution to the wave propagation since the remaining field components are given by equations (1.38).

Examining equation (1.47), it becomes evident that if the frequency falls below a certain *cutoff frequency*,

$$f_{mn} \equiv \frac{c}{2} \sqrt{\left(\frac{m}{a}\right)^2 + \left(\frac{n}{b}\right)^2}, \quad (1.52)$$

the wavenumber becomes imaginary. This signifies that the wave cannot propagate and instead decays exponentially within the waveguide. Such solutions are referred to as *evanescent waves*. This cutoff frequency depends on the mode numbers (m, n) and the dimensions of the waveguide (a, b) . Modes having the same cutoff frequency are called *degenerate*.

The wavelength corresponding to wavenumber k in the direction of guided wave propagation is called the *guide wavelength* and is given by

$$\lambda_g \equiv \frac{2\pi}{k} = \frac{\lambda}{\sqrt{1 - \left(\frac{f_{mn}}{f}\right)^2}} = \frac{\lambda}{\sqrt{1 - \left(\frac{\lambda}{\lambda_{mn}}\right)^2}}. \quad (1.53)$$

This guide wavelength is related to the free-space wavelength, λ , and the cutoff wavelength, λ_{mn} , for the TE_{mn} mode.

To do: Maybe add some talk about modes to finish the theoretical chapter smoothly. Perhaps something about frequency dependence of modes' evanescence or something along the lines of that...

Chapter 2

Polarizer

The design process of a waveguide polarizer is detailed in this chapter. An initial survey of existing literature, including relevant conference papers and research articles, is undertaken. Based on this survey, the performance characteristics of various design concepts are compared and contrasted. A solution to the design problem is then proposed, with a rationale provided for the selected approach. Following this selection, an in-depth eigenmode analysis of the chosen structure is performed. This analysis, as will be demonstrated in this chapter, yields crucial insights into the operational principles, allows for the recognition of key performance parameters, and provides the foundation for the definition of the optimization problem. The chosen structure is subsequently implemented and optimized within CST Studio Suite for a specified target frequency band. The inherent trade-offs between key performance parameters are then discussed, with reference to established principles of guided wave propagation in rectangular waveguides. Finally, the simulated performance of the designed component is presented graphically, derived from full-wave simulations.

2.1 Principle of operation

To achieve dual polarization, the inherent characteristics of symmetric waveguides are leveraged. This choice stems from their unique ability to enable independent control over two orthogonal polarization states possessing identical propagation characteristics. Such independent control is essential for polarization manipulation, allowing for the adjustment of the relative phase and amplitude of these orthogonal modes to achieve the desired polarization states. This capability is directly applied in the design of the dual linear-to-circular polarizer detailed herein. The desired polarization states of RHCP and LHCP were mathematically elaborated on in section 1.2.1.

This crucial characteristic arises from two fundamental properties rooted in the electrodynamics of symmetric waveguides. Firstly, their geometric symmetry (manifesting as mirror or rotational symmetry) permits the existence of two fundamental degenerate modes. A rectangular waveguide, as illustrated in example 1.2.7, exhibits this with its TE₁₀ and TE₀₁ modes. Secondly, as detailed in remark 1.2.6, a fundamental principle derived from Maxwell's equations dictates that any two distinct modes within a waveguide are orthogonal. This orthogonality, expressed mathematically in equation (1.40), ensures that the power flow associated with the interaction of any two distinct modes is zero. In essence, transverse symmetry enables the existence of orthogonally polarized modes, while their inherent orthogonality guarantees their independent propagation without coupling or interference.

The description of circular polarization expressed compactly in equation (1.31) establishes a clear objective for the design of a waveguide polarizer: the creation of a segment, based on a symmetrical waveguide, that introduces a one-quarter wavelength phase difference between the two orthogonal modes along its length, while maintaining equal magnitudes. In subsequent design stages, this latter criterion is quantified by a singular metric known as the *axial ratio* of the emitted wave, which characterizes the polarization purity based on its far-field properties. Several widely adopted approaches exist for achieving these objectives; these may be referred to as standard methods. Notable examples include the following:

- *Dielectric vane polarizers* utilize a dielectric element (a so-called quarter-wave plate) inserted into a segment of a symmetrical waveguide at an angle of $\pm 45^\circ$ relative to the incident electric field. The inserted dielectric introduces a difference in the propagation velocities of the two orthogonal modes along this segment. This differential propagation velocity arises from the interaction of one mode with the vane, which reduces its propagation velocity due to its parallel orientation relative to the vane, while the orthogonal mode remains unaffected due to its perpendicular orientation.
- *Septum polarizers* comprise two rectangular ports converging at a stepped septum and extending into a symmetrical waveguide. When the structure is excited through one of these ports, the septum polarizer converts approximately half of the incident energy to the orthogonal polarization, achieving circular polarization through the introduction of a one-quarter wavelength phase shift at the output port. Excitation of the structure through the alternate port results in circular polarization of the opposite handedness.
- *Iris polarizers* utilize symmetrical waveguides with non-trivial cross-sections, incorporating ridges, also referred to as corrugations or irises, typically positioned symmetrically on two opposing sides. These polarizers operate on a linearly polarized wave incident diagonally into the waveguide. In this configuration, the ridges present inductive characteristics to one of the waveguide modes and capacitive characteristics to the orthogonal mode. This differential interaction results in a one-quarter wavelength phase delay at the output port.

2.2 Literature survey

While the methods established above can be refined and adjusted to achieve favourable results in typical metrics for linear-to-circular polarizers, each also exhibits inherent limitations. Dielectric vane polarizers, while simple to implement, are known to encounter narrow bandwidth issues and suffer from significant power limitations due to inherent dielectric losses. The dielectric losses are encompassed in equation (1.15) as any real dielectric exhibits a small but non-zero conductivity $\sigma > 0$. These losses become particularly pronounced at higher frequencies and power levels, restricting their applicability in certain scenarios. In contrast, septum polarizers offer promising capabilities for a wide range of applications, particularly in terms of power handling and the efficient generation of both right-hand and left-hand circular polarizations. As noted by [6] modifications to septum designs, such as the integration of RF MEMS switches, can achieve reconfigurability and control over the handedness of the produced circular polarization elegantly. However, the size and weight of septum structures can pose significant constraints, especially in compact or weight-sensitive applications.

Furthermore, as highlighted by [7], alternative septum geometries, such as tapered slots, while offering potential design variations, do not necessarily demonstrate substantial performance improvements over conventional stepped septum designs. Iris polarizers, while capable of converting linearly polarized input into both circular polarizations and operating at higher power levels, often exhibit challenges related to ‘overmoding’ within their structures, necessitating precise mode-matching to maintain a satisfactory axial ratio across a broad frequency band. As observed by [8], variations in iris design, such as incorporating ridges on four sides instead of two, can be explored. Moreover, as emphasized by [9], the design of iris arrays requires extensive analysis of the optimal geometry, often involving complex mathematical techniques, to achieve desired performance characteristics. This complexity is further compounded when considering wider bandwidth operation, as noted by [10], which may necessitate cascading individual sections and careful consideration of different ridge types and transmission matrix approaches. Finally, as demonstrated by [11], innovative manufacturing techniques, such as additive manufacturing, combined with alternative waveguide geometries like triangular waveguides, offer potential avenues for further advancement in polarizer design, encompassing design, manufacturing, and measurement aspects.

Departing from these standard methods, various waveguide geometries can be employed for electromagnetic wave manipulation. While standard rectangular and circular waveguides are commonplace, specialized applications such as polarization control often necessitate the use of waveguides with modified cross-sections to introduce a controlled phase difference between orthogonal modes, thereby achieving the desired polarization state. Two prominent examples of such modified waveguides include elliptical waveguides and waveguides with shaped metallic inserts. Elliptical waveguides, as demonstrated in [12] in the context of a wideband circularly polarized horn antenna, leverage their inherent anisotropy to induce the required phase shift. The use of tapered elliptical waveguides, as also explored in [12], facilitates wideband operation. Waveguides with shaped metallic inserts, on the other hand, introduce field perturbations to achieve the desired polarization transformation. As shown in [13]–[16], these inserts can take various forms, including square or triangular blocks inserted into diagonally opposite corners of a square waveguide. This configuration, as validated in [13] and [14], introduces a shorter electrical path for one mode, resulting in a phase delay along the polarizer’s length. Furthermore, as explored in [17], more optimal cross-sectional shapes, such as a bow-tie configuration, can enhance performance, although often at the expense of increased manufacturing complexity. While the higher frequency regions targeted in most of the explored articles are not the primary focus of this work, the underlying principles of achieving polarization control through modified waveguide cross-sections provide valuable insights and inspiration for the design of the polarizer presented herein.

Selected approach. This thesis introduces a novel approach to achieving enhanced polarization purity by employing a straightforward and robust cross-sectional geometry. This geometry is realized by inserting simple prisms into two opposing sides of a waveguide’s cross-section. Initially, both square and circular waveguides, each suitable for dual linear-to-circular polarization conversion, are examined and compared to determine the more advantageous geometry. For the square waveguide illustrated in figure 2.1a, triangular prisms are inserted into two opposing corners, forming a hexagonal waveguide as seen in [14], while circular segments are used for the circular waveguide in figure 2.1b. This concept is inspired by the established technique of chamfering opposing corners of a circularly polarized patch antenna. The resulting waveguide structures can

be considered Babinet-complementary¹ to this antenna configuration.

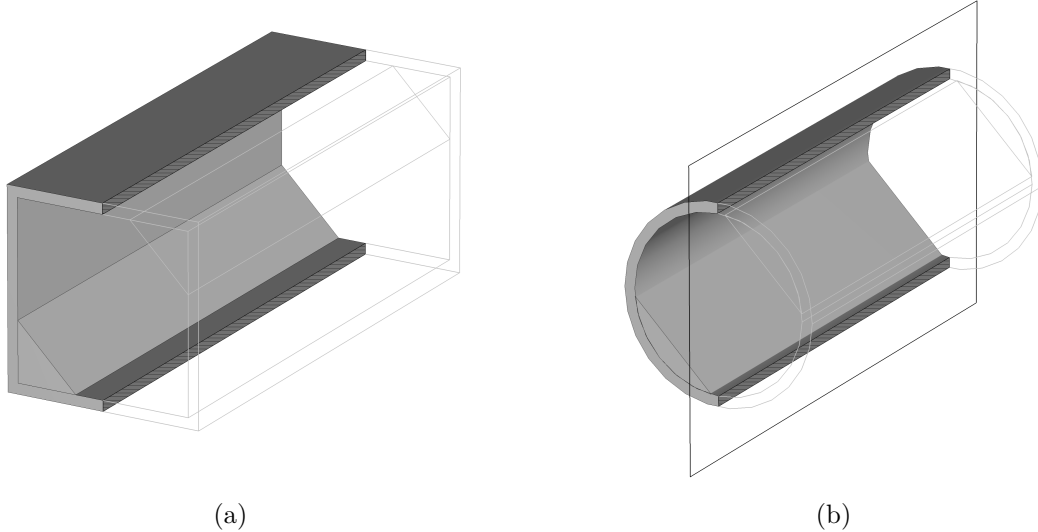


Figure 2.1: Polarizers based on symmetric waveguides

This approach was selected primarily for its relative ease of fabrication, particularly at higher frequencies, and its potential for adaptation to various frequency bands. However, due to the resonant, and hence geometry-dependent, nature of the mode dispersion introduced by the prismatic inserts, optimal performance is anticipated over a moderately wide bandwidth, rather than an ultrawide one. This bandwidth limitation represents a trade-off for the design's simplicity, robustness, and manufacturability. The use of triangular prisms, in particular, simplifies fabrication compared to more complex curved geometries while still providing effective field manipulation for polarization control.

2.3 Eigenmode analysis

The focus now shifts to the *eigenmode analysis* the two waveguides illustrated in figure 2.1. This powerful technique, based on the theory outlined in remark 1.2.6, facilitates the establishment of figures of merit intrinsic to polarizing structures, enabling performance tracking and aiding in the determination of the more advantageous geometry.

Initially, the fundamental modes of propagation in the symmetric waveguides, *without* the inserted prisms, are considered. In the case of the square waveguide, it is the TE₁₀ and TE₀₁ modes illustrated in figures 2.2a and 2.2b, whereas the two degenerate TE₁₁ modes² of the circular waveguide are presented in figures 2.2c and 2.2d. For both waveguides individually, these two degenerate modes represent the two waves launched into the polarizer via a section of standard waveguide. Upon encountering the metallic inserts, such incident wave no longer represents the eigenmode of the simple waveguide structure and its energy is coupled into a linear combination of the fundamental eigenmodes of the respective polarizer.

¹This name refers to the notion of complementary structures according to *Babinet's principle*, derivation of which is out of scope for this text. More details can be found, e.g., in [18].

²Note that circular waveguides possess an infinite number of degenerate TE₁₁ modes due to their rotational symmetry. Here, two are chosen for their perpendicular oscillations which aligns well with the definition of circular polarization in section 1.2.3.

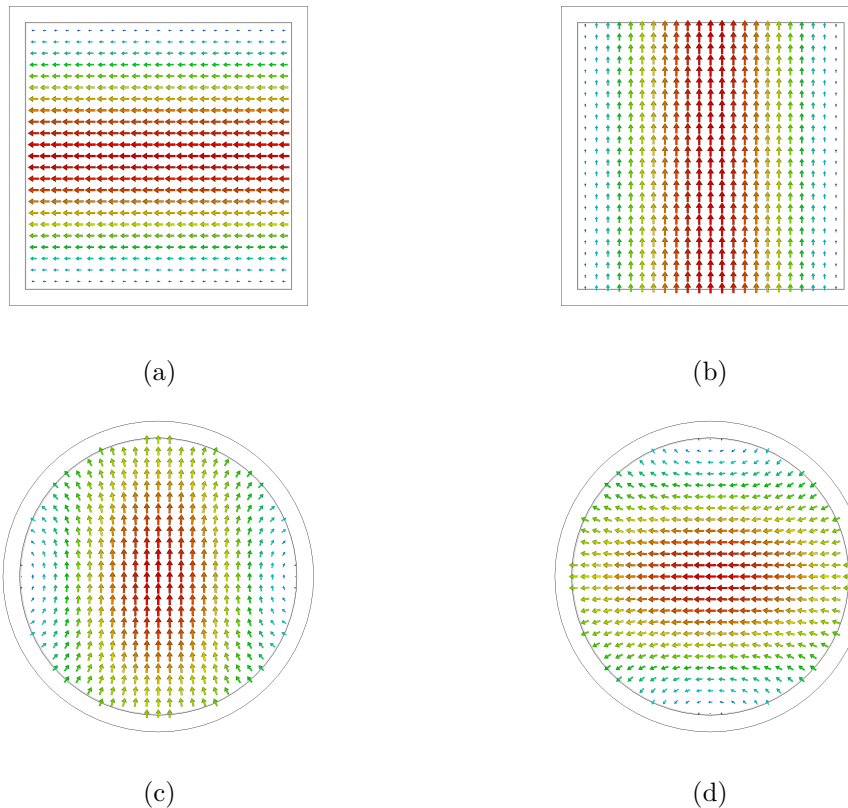


Figure 2.2: Fundamental modes of the symmetric waveguides

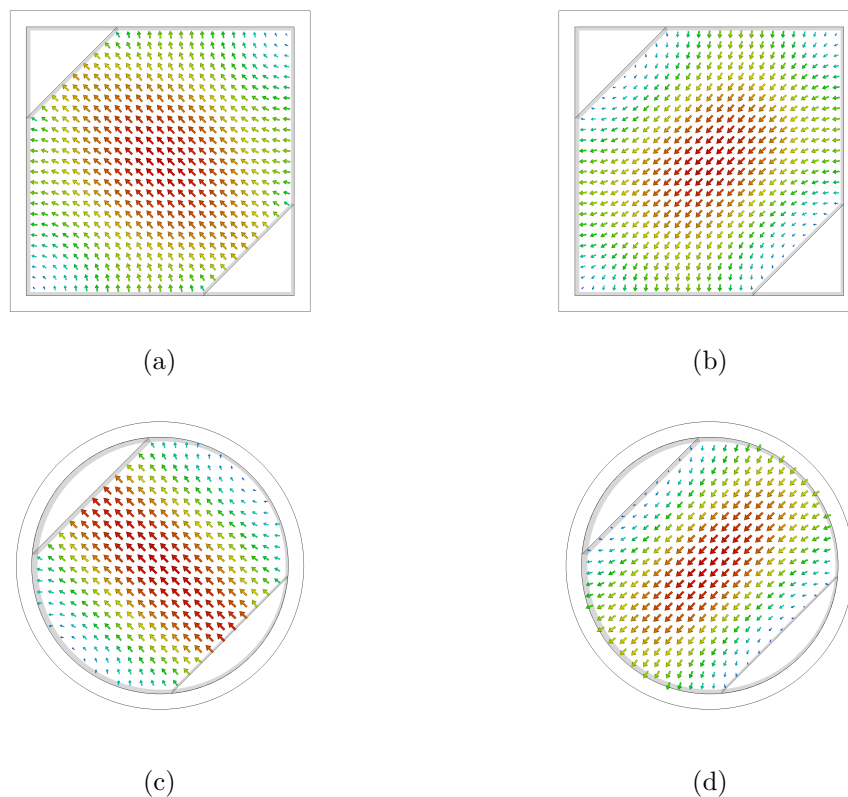


Figure 2.3: Fundamental modes of the symmetric waveguides with metallic inserts

With the basic modes established, the eigenmodes of the polarizers, i.e., the same waveguides but now *with* the prisms inserted, are analysed. The eigenmodes take the form presented in figures 2.3a and 2.3b for the square geometry, whereas the circular waveguide with inserts supports two fundamental modes depicted in figures 2.3c and 2.3d. As expected, in both cases, the transverse field exhibits a standing wave behaviour as dictated by the boundary conditions on a conductive surface. More importantly for the polarization transformation, the prisms perturb the electromagnetic fields, leading to a change in the propagation constants of the existing modes. Crucially, the presence of these inserts breaks the original symmetry of the waveguide, causing a dispersion, or difference in phase velocity, between the two fundamental modes of propagation. This fact is illustrated in figure 2.3, where in both geometries, one of the modes perceives a different electric path than the other. This dispersion is the key mechanism for achieving circular polarization. As the electromagnetic wave propagates along the waveguide, the phase difference between the two fundamental modes accumulates. By carefully selecting the geometry and placement of the inserts, as well as the length of the waveguide, this cumulative phase lag can be precisely controlled. In the context of a polarizer designed to generate circular polarization, the goal is to achieve exactly one-quarter wavelength phase difference between the two modes at the output. As shown in equation (1.31), this quadrature phase relationship, combined with equal amplitudes of the two modes, results in the generation of a circularly polarized wave. The eigenmode analysis allows for the accurate determination of the modal field distributions, enabling precise design and optimization of the polarizer to achieve the desired phase shift and polarization state.

Remark 2.3.1 [Dual polarization capability]. It is important to note that, with respect to the diagonal symmetry of the polarizer, one of its eigenmodes is always antisymmetric. This means that if exciting the square-waveguide-based polarizer with the TE₀₁ results in a RHCP, the TE₁₀ must result in LHCP, or vice versa. This principle can be visualized as decomposing the incident waves from figures 2.2a and 2.2b into the basis formed by polarizer eigenmodes depicted in figures 2.3a and 2.3d: While the horizontal waveguide mode (figure 2.2a) can be expressed as a simple sum of the two polarizer modes, the vertical waveguide mode (figure 2.2b) requires the negative³ of the antisymmetric polarizer mode (figure 2.3b). Although this principle was illustrated using the square waveguide structure, the same holds true for the circular geometry with its two orthogonal degenerate modes (figures 2.2c and 2.2d). This unique property enables the structures to produce dual circular polarization simply by switching between two excitations.

Furthermore, due to the mirror symmetry of both polarizers, optimizing the structure with respect to just a single orientation of circular polarization is sufficient. By the essence of the matter, the other polarization must retain the same performance parameters, as will be proven by simulation.

2.3.1 Figures of merit

A crucial outcome of the eigenmode analysis is the gained insight into the operational principles, which helps define relevant variables and performance parameters

³A positive sum of the two eigenmodes is equivalent to the plus sign option in equation (1.32), as the condition on circular polarization expressed in equation (1.31) is fulfilled due to the two eigenmodes oscillating perpendicular to each other, i.e., $\delta = \pi/2$. Conversely, adding one eigenmode to the negative of the other introduces an additional π to the phase difference δ . The condition for circular polarization is again fulfilled, but with $\delta = 3\pi/2$, causing the sine in equation (1.32) to take a negative value, resulting in the opposite circular polarization.

intrinsic to the structure's geometry, ultimately aiding in polarizer optimization. The optimization process aims to produce circular polarization while minimizing production costs, primarily by reducing the polarizer length, L . This necessitates maximizing the *specific mode phase shift*, given by

$$\Delta k_L(f) = \frac{1}{L} \int_0^L [k_2 - k_1](z, f) dz, \quad (2.1)$$

where k_1 and k_2 are the propagation constants of the two polarizer modes and z is the Cartesian coordinate aligned with the propagation direction. This quantity represents the average difference in propagation constants between the two modes along the polarizer,⁴ effectively quantifying the rate at which the phase difference between them accumulates as they propagate. However, equation (2.1) addresses only one of the two conditions for circular polarization (1.31), the other being the requirement for equal mode amplitudes:

$$\left. \frac{E_2}{E_1} \right|_{z=L} = 1, \quad (2.2)$$

where E_1 and E_2 are the amplitudes of the two modes and the polarizer output. A weighted aggregate of equations (2.1) and (2.2) forms the objective function of the optimization problem, with the variables being the geometric parameters of the polarizer cross-section. Intuitively, larger inserted prisms induce a greater phase lag per unit length but also introduce larger amplitude distortions between the modes. This reveals an inherent conflict within the problem, necessitating a trade-off. From an application perspective, a balance must be struck between the length of the structure, which compensates for a lower phase delay per unit length, and polarization purity, which is compromised by unequal mode magnitudes.

Let's draft up some numbers for the geometries and compare the polarizer geometries. Also simplify equation (2.1) and talk about how we extract both metrics in CST.

2.3.2 Comparison of symmetric waveguides

To conclude the eigenmode analysis, a determination will be made, using the previously introduced figures of merit, regarding which geometry is better suited for polarization control, considering both practical and performance aspects. Ideally, minimal frequency dependence of both figures, equations (2.1) and (2.2), is desired. However, due to the inherently resonant operational principle of the waveguide, achieving feasible performance across an ultrawide band with a single section of such a polarizing structure is not considered possible.

Before proceeding, the practical evaluation of equations (2.1) and (2.2) should be addressed. Given that both polarizers are analysed as uniform waveguides (figures 2.1a and 2.1b), the propagation dispersion between the two modes, and consequently both metrics, can be approximated as constant throughout the polarizer. This approximation allows equation (2.1) to be expressed as

$$\Delta k_L(f) = [k_2 - k_1](f) \quad (2.3)$$

⁴This quantity is analogous to the birefringence effect observed in optics, where a material exhibits different refractive indices for different polarizations, causing a phase difference to accumulate between them as they propagate. Here, the waveguide structure, due to its geometry, effectively creates different propagation constants for the two orthogonal modes, leading to a similar effect.

and the overall mode phase shift at the polarizer output is given by

$$\Delta\phi(f) = L [k_2 - k_1](f). \quad (2.4)$$

Furthermore, this simplification permits the evaluation of both equations (2.2) and (2.3) from a single reading at the polarizer output. For this purpose, an *E-field probe* functionality within CST Studio Suite can be utilized, allowing the magnitude and phase of the electric field to be determined at a specified point in space, evaluated across all frequencies. Consequently, the objective function for maximum specific phase shift, equation (2.1), is transformed into the minimization of

$$L_{\perp}(f) = \frac{\pi}{4} \frac{L}{\Delta\phi}(f) \quad (2.5)$$

representing the polarizer length required to achieve a mode phase shift of $\pi/4$.⁵ This modified objective function can be readily computed using the *Template-Based Post-Processing* feature within CST Studio Suite, using $\Delta\phi(f)$ obtained from the E-field probe result. Moreover, the practical feasibility of the polarizer is inherently incorporated into this formulation.

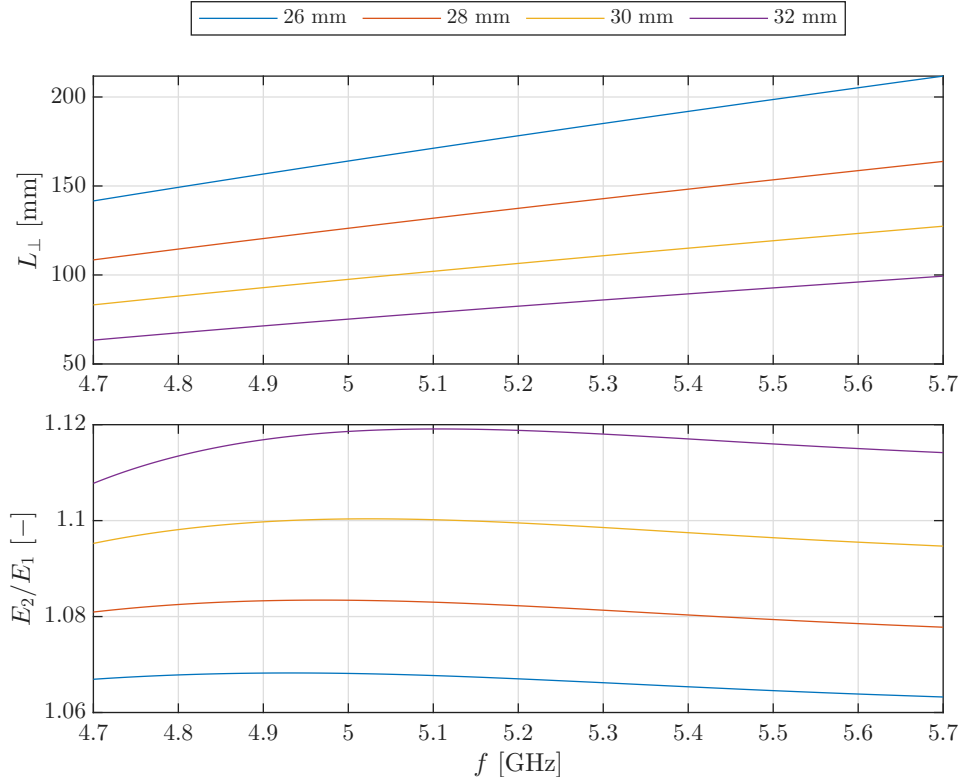


Figure 2.4: Circular polarizer cross-section

⁵It is important to note that, due to phase wrapping, the cross-section tuning simulations must be conducted for a polarizer shorter than that required to produce a $\pi/4$ phase shift.

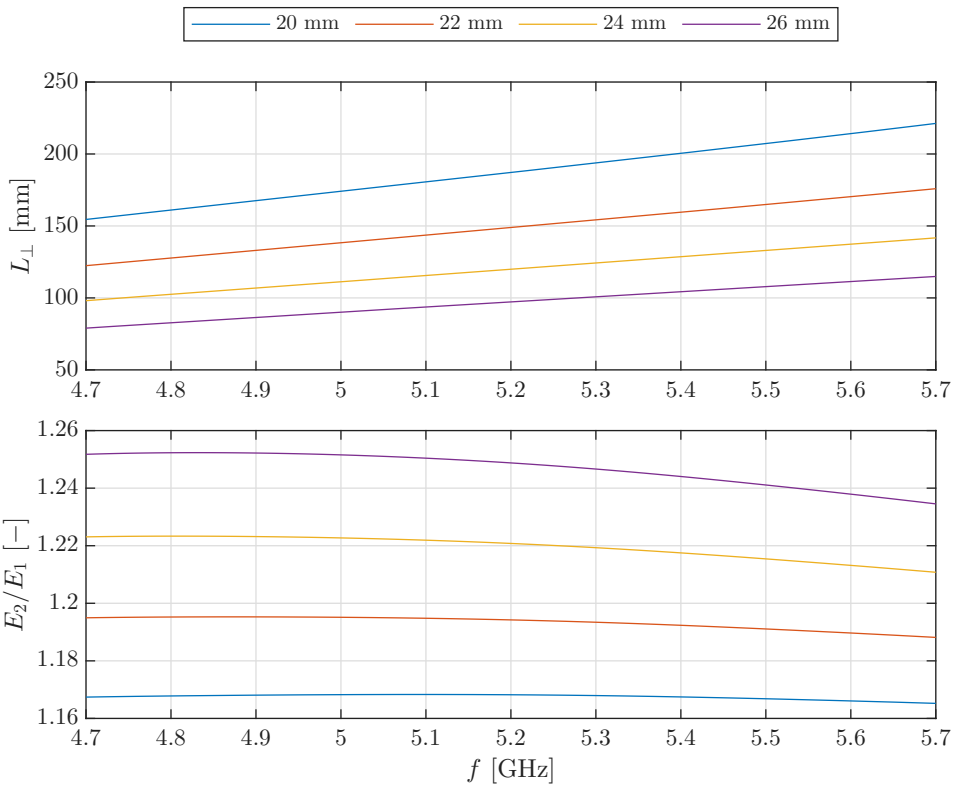


Figure 2.5: Square polarizer cross-section

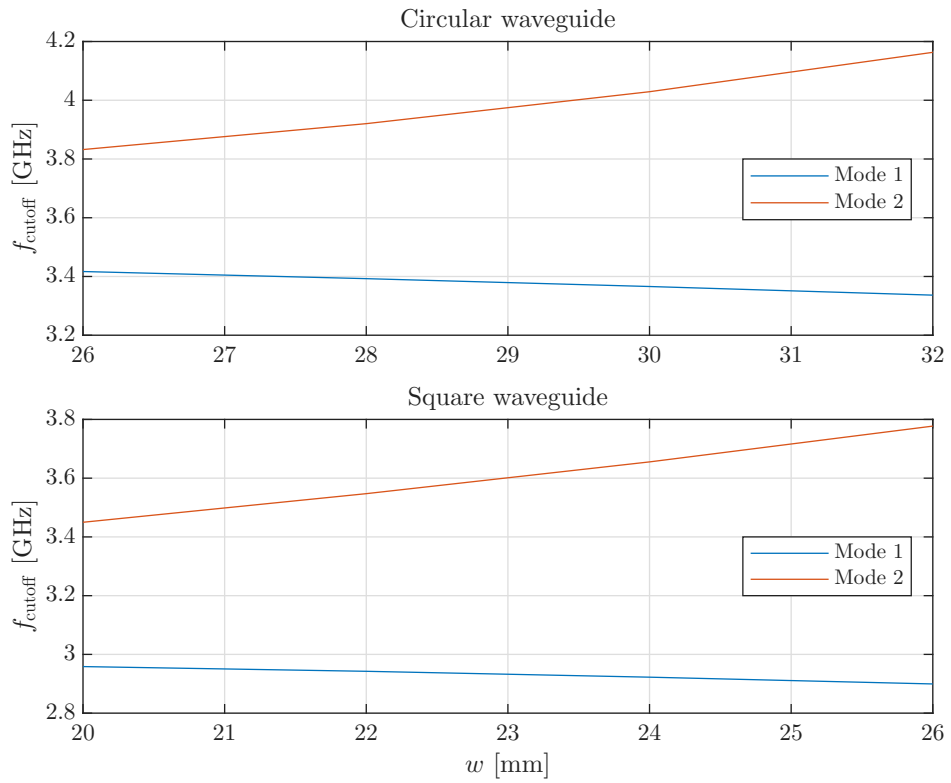


Figure 2.6: Polarizers – cutoff frequencies

2.4 Square waveguide polarizer

2.4.1 Selection of parameters

Frequency band, reference commercial waveguide for recommended band, side length determination, polarizer length determination, ...

2.4.2 Cross-section tuning

Trade-off: unit mode amplitude ratio vs. high mode phase lag per unit length, ...

2.5 Simulation results

Add text, ...

2.5.1 Waveguide feed simulation

Exciting the structure with a waveguide feed with two modes, mode metrics ...

2.5.2 Radiation properties

Using open-ended waveguide, ...

Chapter 3

Feeding structure

3.1 Coaxial-to-waveguide transition

Single feed, dual feed from [19], ...

3.2 Dual feed

Add text, ...

3.2.1 Single feed

Right-angle transition, simulation boundary consideration, effects of individual parameters, optimization, ...

3.2.2 Grating

Isolation of optimization variables, reflection vs. cross-talk minimization trade-off, ...

3.2.3 Dual feed optimization

Initial results, optimization script, ...

Chapter 4

Antenna

Add text including target gain

4.1 Conical horn

Theoretical guidelines from [20], Antenna Magus, adaptation of a conical horn to a square waveguide ...

4.2 Simulation results

Design using Antenna Magus, effects of individual parameters when adapting the geometry, ...

Chapter 5

Assembly

Add text, ...

5.1 First results

The tragic results, analysis, ...

5.2 Grating removal

Decision reasoning, lack of grating's meaning, ...

5.3 Product finalization

Tuning results vs. optimization, fine-mesh and high-precision verifications, practical assembly adjustments by UMT, ...

5.4 Measurement results

Comparison of measurement results with simulation data, ...

Conclusion

Suspendisse vitae elit. Aliquam arcu neque, ornare in, ullamcorper quis, commodo eu, libero. Fusce sagittis erat at erat tristique mollis. Maecenas sapien libero, molestie et, lobortis in, sodales eget, dui. Morbi ultrices rutrum lorem. Nam elementum ullamcorper leo. Morbi dui. Aliquam sagittis. Nunc placerat. Pellentesque tristique sodales est. Maecenas imperdiet lacinia velit. Cras non urna. Morbi eros pede, suscipit ac, varius vel, egestas non, eros. Praesent malesuada, diam id pretium elementum, eros sem dictum tortor, vel consectetur odio sem sed wisi.

Sed feugiat. Cum sociis natoque penatibus et magnis dis parturient montes, nascetur ridiculus mus. Ut pellentesque augue sed urna. Vestibulum diam eros, fringilla et, consectetur eu, nonummy id, sapien. Nullam at lectus. In sagittis ultrices mauris. Curabitur malesuada erat sit amet massa. Fusce blandit. Aliquam erat volutpat. Aliquam euismod. Aenean vel lectus. Nunc imperdiet justo nec dolor.

Etiam euismod. Fusce facilisis lacinia dui. Suspendisse potenti. In mi erat, cursus id, nonummy sed, ullamcorper eget, sapien. Praesent pretium, magna in eleifend egestas, pede pede pretium lorem, quis consectetur tortor sapien facilisis magna. Mauris quis magna varius nulla scelerisque imperdiet. Aliquam non quam. Aliquam porttitor quam a lacus. Praesent vel arcu ut tortor cursus volutpat. In vitae pede quis diam bibendum placerat. Fusce elementum convallis neque. Sed dolor orci, scelerisque ac, dapibus nec, ultricies ut, mi. Duis nec dui quis leo sagittis commodo.

Aliquam lectus. Vivamus leo. Quisque ornare tellus ullamcorper nulla. Mauris porttitor pharetra tortor. Sed fringilla justo sed mauris. Mauris tellus. Sed non leo. Nullam elementum, magna in cursus sodales, augue est scelerisque sapien, venenatis congue nulla arcu et pede. Ut suscipit enim vel sapien. Donec congue. Maecenas urna mi, suscipit in, placerat ut, vestibulum ut, massa. Fusce ultrices nulla et nisl.

Glossary of Symbols

ϵ	permittivity
μ	permeability
$\partial\Omega$	boundary of set Ω
∂_ξ	partial derivative w.r.t. variable ξ
ρ_e	electric charge density
ρ_m	magnetic charge density
σ	conductivity
B	magnetic field
D	auxiliary electric field
E	electric field
e_ξ	unit vector in the ξ -direction
e_n	polarization vector
H	auxiliary magnetic field
J_e	electric current density
J_m	magnetic current density
k	wave vector

Bibliography

- [1] C. Balanis, *Advanced Engineering Electromagnetics*. Wiley, 2012, ISBN: 9781118213483. [Online]. Available: <https://books.google.com.tw/books?id=2eMbAAAAQBAJ>.
- [2] D. Griffiths, *Introduction to Electrodynamics* (Pearson international edition). Prentice Hall, 1999, ISBN: 9780139199608. [Online]. Available: <https://books.google.com.tw/books?id=x0akQgAACAAJ>.
- [3] A. Zangwill, *Modern Electrodynamics* (Modern Electrodynamics). Cambridge University Press, 2013, ISBN: 9780521896979. [Online]. Available: <https://books.google.com.tw/books?id=tEYSUegp9WYC>.
- [4] E. Titchmarsh, *Introduction to the Theory of Fourier Integrals*. Clarendon Press, 1948, ISBN: 9780608133492. [Online]. Available: <https://books.google.com.tw/books?id=1BMIAQAAIAAJ>.
- [5] A. Oppenheim, A. Willsky and S. Nawab, *Signals & Systems* (Prentice-Hall signal processing series), 2nd ed. Prentice-Hall International, 1997, ISBN: 9780136511755. [Online]. Available: <https://books.google.com.tw/books?id=09ZHSAAACAAJ>.
- [6] J. A. Ruiz-Cruz, M. M. Fahmi, M. Daneshmand and R. R. Mansour, ‘Compact reconfigurable waveguide circular polarizer,’ in *2011 IEEE MTT-S International Microwave Symposium*, Baltimore, MD, USA, 2011, pp. 1–4. DOI: [10.1109/MWSYM.2011.5972872](https://doi.org/10.1109/MWSYM.2011.5972872).
- [7] X. Wang, X. Huang and X. Jin, ‘Novel square/rectangle waveguide septum polarizer,’ in *2016 IEEE International Conference on Ubiquitous Wireless Broadband (ICUWB)*, Nanjing, China, 2016, pp. 1–4. DOI: [10.1109/ICUWB.2016.7790510](https://doi.org/10.1109/ICUWB.2016.7790510).
- [8] H. Song, L. Jia, J. Tan, Y. Zhang and S. Liu, ‘Design of wideband quad-ridge waveguide polarizer,’ in *2023 4th China International SAR Symposium (CISS)*, Xian, China, 2023, pp. 1–6. DOI: [10.1109/CISS60136.2023.10379971](https://doi.org/10.1109/CISS60136.2023.10379971).
- [9] G. Vironi, R. Tascone, O. A. Peverini and R. Orta, ‘Optimum-iris-set concept for waveguide polarizers,’ *IEEE Microwave and Wireless Components Letters*, vol. 17, no. 3, pp. 202–204, Mar. 2007. DOI: [10.1109/LMWC.2006.890474](https://doi.org/10.1109/LMWC.2006.890474).
- [10] S. Piltyay, A. Bulashenko, H. Kushnir and O. Bulashenko, ‘New tunable iris-post square waveguide polarizers for satellite information systems,’ in *2020 IEEE 2nd International Conference on Advanced Trends in Information Theory (ATIT)*, Kyiv, Ukraine, 2020, pp. 342–348. DOI: [10.1109/ATIT50783.2020.9349357](https://doi.org/10.1109/ATIT50783.2020.9349357).
- [11] B. Deutschmann and A. F. Jacob, ‘Broadband septum polarizer with triangular common port,’ *IEEE Transactions on Microwave Theory and Techniques*, vol. 68, no. 2, pp. 693–700, Feb. 2020. DOI: [10.1109/TMTT.2019.2951138](https://doi.org/10.1109/TMTT.2019.2951138).
- [12] H.-Y. Yu, J. Yu, X. Liu, Y. Yao and X. Chen, ‘A wideband circularly polarized horn antenna with a tapered elliptical waveguide polarizer,’ *IEEE Transactions on Antennas and Propagation*, vol. 67, no. 6, pp. 3695–3703, Jun. 2019. DOI: [10.1109/TAP.2019.2905789](https://doi.org/10.1109/TAP.2019.2905789).

- [13] L. A. Rud and K. S. Shpachenko, ‘Polarizers on sections of square waveguides with inner corner ridges,’ in *2011 VIII International Conference on Antenna Theory and Techniques*, Kyiv, Ukraine, 2011, pp. 338–340. DOI: [10.1109/ICATT.2011.6170775](https://doi.org/10.1109/ICATT.2011.6170775).
- [14] S. Bhardwaj and J. Volakis, ‘Hexagonal waveguides: New class of waveguides for mm-wave circulaly polarized horns,’ in *2018 International Applied Computational Electromagnetics Society Symposium (ACES)*, Denver, CO, USA, 2018, pp. 1–2. DOI: [10.23919/ROPACES.2018.8364165](https://doi.org/10.23919/ROPACES.2018.8364165).
- [15] S. Bhardwaj and J. L. Volakis, ‘Hexagonal waveguide based circularly polarized horn antennas for sub-mm-wave/terahertz band,’ *IEEE Transactions on Antennas and Propagation*, vol. 66, no. 7, pp. 3366–3374, Jul. 2018. DOI: [10.1109/TAP.2018.2829842](https://doi.org/10.1109/TAP.2018.2829842).
- [16] S. Bhardwaj and J. L. Volakis, ‘Circularly-polarized horn antennas for terahertz communication using differential-mode dispersion in hexagonal waveguides,’ in *2017 IEEE International Symposium on Antennas and Propagation & USNC/URSI National Radio Science Meeting*, San Diego, CA, USA, 2017, pp. 2571–2572. DOI: [10.1109/APUSNCURSINRSM.2017.8073328](https://doi.org/10.1109/APUSNCURSINRSM.2017.8073328).
- [17] E. Garcia-Marin, J. L. Masa-Campos, P. Sanchez-Olivares and J. A. Ruiz-Cruz, ‘Bow-tie-shaped radiating element for single and dual circular polarization,’ *IEEE Transactions on Antennas and Propagation*, vol. 68, no. 2, pp. 754–764, Feb. 2020. DOI: [10.1109/TAP.2019.2943357](https://doi.org/10.1109/TAP.2019.2943357).
- [18] M. Born, E. Wolf and A. Bhatia, *Principles of Optics: Electromagnetic Theory of Propagation, Interference and Diffraction of Light*. Cambridge University Press, 1999, ISBN: 9780521642224. [Online]. Available: <https://books.google.com.tw/books?id=nUHGpfNsGyUC>.
- [19] S. K. Karki, J. Ala-Laurinaho and V. Viikari, ‘Dual-polarized probe for planar near-field measurement,’ *IEEE Antennas and Wireless Propagation Letters*, vol. 22, no. 3, pp. 576–580, Mar. 2023. DOI: [10.1109/LAWP.2022.3218731](https://doi.org/10.1109/LAWP.2022.3218731).
- [20] N. A. Aboserwal, C. A. Balanis and C. R. Birtcher, ‘Conical horn: Gain and amplitude patterns,’ *IEEE Transactions on Antennas and Propagation*, vol. 61, no. 7, pp. 3427–3433, Jul. 2013. DOI: [10.1109/TAP.2013.2256453](https://doi.org/10.1109/TAP.2013.2256453).

Index

- boundary conditions, 8
- circular polarization, 13
- constitutive parameters, 7
- constitutive relations, 7
- cutoff frequency, 17
- degenerate modes, 17
- elliptical polarization, 12
- guide wavelength, 17
- Helmholtz equations, 14
- linear polarization, 12
- modal decomposition, 16
- monochromatic plane wave, 9
- polarization vector, 11